Running Title: Immunoglobulin M regulates airway hyperresponsiveness independent of T helper 2 allergic inflammation.

Authors and Affiliations:

Sabelo Hadebe[a*], Anca Flavia Savulescu[b], Jermaine Khumalo[a], Katelyn Jones[a], Sandisiwe Mangali[a,c], Nontobeko Mthembu[a], Fungai Musaigwa[a], Welcome Maepa[b], Hlumani Ndlovu[b], Amkele Ngomti[a,] Martyna Scibiorek[a,c], Javan Okendo[b,e], Frank Brombacher[a,c,d*]

[a]Division of Immunology, and South African Medical Research Council (SAMRC) Immunology of Infectious Diseases, Department of Pathology, Faculty of Health Sciences, University of Cape Town, Cape Town, South Africa

[b]Division of Chemical, Systems & Synthetic Biology, Faculty of Health Sciences, Institute of Infectious Disease & Molecular Medicine, University of Cape Town, Cape Town, South Africa

[c]International Centre for Genetic Engineering and Biotechnology (ICGEB) and Institute of Infectious Diseases and Molecular Medicine (IDM), Division of Immunology, Health Science Faculty, University of Cape Town, Cape Town, South Africa

[d]Wellcome Centre for Infectious Diseases Research in Africa (CIDRI-Africa), Institute of Infectious Diseases and Molecular Medicine (IDM), Faculty of Health Sciences, University of Cape Town, Cape Town, 7925, South Africa

[e]Centre for Research in Therapeutic Sciences (CREATES), Strathmore University, Nairobi, Kenya

* **Corresponding Author**: Professor Frank Brombacher

International Centre for Genetic Engineering and Biotechnology (ICGEB) and Institute of

Infectious Diseases and Molecular Medicine (IDM), Division of Immunology, Health Science

Faculty, University of Cape Town, Cape Town, South Africa

Email: brombacherfrank@gmail.com

Tel: +27 21 406 6424

Fax: +27 21 406 6938

* **Corresponding author:** Dr Sabelo Hadebe

Division of Immunology, Health Science Faculty, University of Cape Town, Cape Town, South Africa

Email: sabelo.hadebe@uct.ac.za

Tel: +27 21 406 6161

Fax: + 27 21 406 6029

Abstract

Allergic asthma is a disease driven by T helper 2 (Th2) cells, eosinophilia, airway hyperresponsiveness (AHR) and IgE-secreting B cells. Asthma is largely controlled by corticosteroids and β_2 adregenic receptor agonists that target and relax airway smooth muscle (ASM). Immunoglobulin M (IgM) isotype secreted by naïve B cells is important for class switching but may have other undefined functions.

We investigated the role of IgM in a house dust mite (HDM)-induced Th2 allergic asthma model.

We sensitised wild-type (WT) and IgM-deficient ($IgM^{-/-}$) mice with HDM and measured AHR, and Th2 responses. We performed RNA sequencing on the whole lung of WT and $IgM^{-/-}$ mice sensitised to saline or HDM. We validated our AHR data on human ASM by deleting genes using CRISPR and measuring contraction by single-cell force cytometry.

We found IgM to be essential in AHR but not Th2 airway inflammation or eosinophilia. RNA sequencing of lung tissue suggested that IgM regulated AHR through modulating brain-specific angiogenesis inhibitor 1-associated protein 2-like protein 1 (*Baiap2l1*) and other genes. Deletion of *BAIAP2L1* led to a differential reduction in human ASM contraction when stimulated with TNF-α and Acetylcholine, but not IL-13.

These findings have implications for future treatment of asthma beyond current therapies.

Keywords: Immunoglobulin M, B cells, airway hyperresponsiveness, airway smooth muscle; TH2 cells; single cell force cytometry; fluorescently labelled elastomeric contractible surface; CRISPR-Cas9; *BAIAP2L1*

INTRODUCTION

Immunoglobulin M (IgM) is the first antibody isotype expressed during B cell development and the first humoral antibody responder, conserved across all species from zebrafish to humans [1]. IgM can be divided into natural and antigen-induced IgM and can either be membrane-bound IgM-type B cell receptor (BCR) or secreted IgM [2,3]. Natural IgM plays multiple roles in homeostasis including scavenging and clearance of apoptotic cell debris in conjunction with phagocytic macrophages, B cell survival through tonic signals, lymphoid tissue architecture and prevention of autoimmune diseases [4–6]. At mucosal sites, both natural and antigen-induced IgM play a role in shaping healthy microbiota and IgM repertoire is also shaped by microbiota [7,8]. Secreted IgM antigen complexes can connect signals via unique and shared receptors, suggestive of a more pleiotropic role in homeostasis and disease states [9–11].

Natural IgM and secreted IgM are essential in many infectious and non-infectious diseases including those induced by parasites, fungi, bacterial, viral and autoimmune diseases [11]. In *Plasmodium falciparum*, anti-α-gal IgM and anti-MSP1 directed antibodies are protective against primary and secondary infections [12,13]. Mice deficient of secreted IgM are susceptible to pulmonary *Cryptococcus neoformans* and *P. carinii* infection partly due to reduced activation of innate and adaptive responses [14,15]. At mucosal surfaces, IgM promotes healthy gut bacteria that is beneficial for homeostasis such as Firmicutes and Bacteroidetes [16]. Natural and induced secreted IgM produced mainly by B1a cells is protective against *Streptococcus pneumoniae* and *Francisella tularensis* infection [17,18]. In these settings, the protective effects of sIgM depended on

cytokines IL-1β and GM-CSF [17,18]. The involvement of natural or induced IgM in allergic asthma is unknown, despite selective IgM syndrome dominated by asthma patients [19].

Asthma is a T helper 2 (Th2) disease characterised by eosinophilic lung inflammation, mucus production, airway hyperresponsiveness (AHR), Th2 cytokines (interleukin-4 (IL-4), IL-5 and IL-13) and B cells producing IgE [20]. IgM is central to class switch recombination that results in IgE class switched B cells [21]. We and others recently showed that that the role of B cells in asthma is complex, where the load of the antigen is crucial in their function [22–24]. Mice deficient of B cells ($\mu MT^{-/-}$) can mount exaggerated AHR when challenged with house dust mite (HDM) [24–26] or ovalbumin (OVA) [27–29] partly due to lack of regulatory B cells that dampen AHR [23]. Furthermore, interleukin 4 receptor alpha signalling in B cells is required for optimal Th2 allergic airway inflammation through regulation of AHR, germinal centre (GC) formation and B effector 2 function [22].

Interestingly, B cell isotypes show unique functions in allergic asthma, for example IgE and its high affinity receptor, FcεR are redundant in an HDM model [30], whereas IgD plays an amplifying and regulatory role in various allergic models [31]. In this context IgD activate basophils to secrete IL-4 and Th2 induction during the sensitisation stage through binding basophils via galectin-9 and CD44. Once Th2 responses have been amplified, IgD ligation blocked IgE-mediated basophil degranulation through competing for antigen and inhibiting FcεR mediated signalling [31]. How IgM isotype contributes in the development of allergic asthma is unclear. It is also unclear whether secreted IgM plays different roles compared to membrane bound IgM, which is more likely to undergo class switching to IgE. We challenged mice lacking both membrane

and secreted IgM with HDM and other allergens and found a profound reduction in AHR. RNA sequencing of lung tissue showed a downregulation of brain-specific angiogenesis inhibitor 1-associated protein 2-like protein 1 (*Baiap2l1*) and erythroid differentiation regulatory factor 1 (*Erdr1*) genes associated with actin cytoskeleton and rearrangement smooth muscle contraction. As a proof of principle, we showed in human smooth muscle cell line that deletion of these genes via CRISPR- resulted in reduction in smooth muscle contraction at a single cell level. These are unexpected functions of secreted, and membrane bound IgM; namely, its involvement in modulating airway smooth muscle contraction.

METHODS

Mice

IgM-deficient homozygotes mice on Balb/C background and on C57BL/6 background were backcrossed at least 10 generations [32]. Wild type on Balb/C and C57BL/6 backgrounds were used as a littermate control. Mice were housed in independently ventilated cages under specific pathogen-free conditions at the University of Cape Town Animal Facility. All mice were used at eight to 10 weeks of age and animal procedures were performed according to the strict recommendation by the South African Veterinary Council and were approved by the University of Cape Town Animal Ethics Committee (Reference number 014/019, 018/013 and 022/014).

House Dust-mite induced allergic airway disease

A high dose and a low dose HDM treatment schedule were used to induce symptoms of allergic asthma in mice [22]. Mice were anaesthetised with ketamine (Anaket-V; Centaur Labs, Johannesburg, South Africa) and xylazine (Rompun; Bayer, Isando, South Africa). For low-dose HDM, mice were sensitised intratracheally (i.t.) on day 0 with 1 µg of HDM (Stellergens Greer Laboratories, Lenoir, U.S.A.) and intranasally challenged with 3 ug HDM on days 8, 9, 10, 11 and 12. For high-dose HDM, mice were with HDM 100 ug and challenged with HDM 10 ug. AHR was measured on day 15. After the procedure, mice were euthanised and tissue samples were collected for analysis.

Adoptive transfer of naïve B cells

Spleens were collected from naïve congenic CD45.1 Balb/C mice and passed through 40µm strainer to obtain single-cell suspensions. Cells were stained with FITC-B220

and APC-CD19 for 30min at 4°C. A dead cell exclusion dye (7AAD) was added before sorting on BD FACS Aria I to at least 96% purity. 2-5 x 10^6 cells were adoptively transferred intravenously (i.v.) into $IgM^{-/-}$ recipient mice a day before HDM sensitisation.

Adoptive transfer of naïve serum

Naïve wild-type mice were euthanised and blood was collected via cardiac puncture before being spun down (5500rpm, 10min, RT) to collect serum. Serum (200μL) was injected intraperitoneally into IgM-deficient mice, 1 day before sensitisation with HDM. In some experiments, serum was injected intraperitoneally at day -1, 0, and a day before challenges.

Ovalbumin-induced allergic airway inflammation

Mice were sensitised intraperitoneally with (50μg in 200μl) of ovalbumin (OVA) adsorbed to 0.65% alum (Sigma-Aldrich, Aston Manor, South Africa) on days 0, 7, 14. On days 23, 24, 25, mice were intranasally challenged with 100μg of OVA under anaesthesia with ketamine (Anaket-V; Centaur Labs, Johannesburg, South Africa) and xylazine (Rompun; Bayer, Isando, South Africa). AHR was measured on day 26. After the procedure, mice were euthanized with halothane and tissue samples collected for analysis.

Papain-induced lung inflammation

Mice were anaesthetized with isoflourane (3L/min) briefly before being challenged with 50μL of 25 μg of Papain (Sigma-Aldrich, Aston Manor, South Africa) on days 1, 2 and

3 or PBS. AHR was measured on day 4. After the procedure, mice were euthanized with halothane and tissue samples collected for analysis.

Airway Hyperresponsiveness

Airway resistance and elastance of the whole respiratory system (airways, lung chest wall) after intranasal challenge was determined by forced oscillation measurements as described previously [33] with the Flexivent system (SCIREQ, Montreal, Canada) by using the single compartment (''snapshot'') perturbation. Measurements were carried out with increasing doses of acetyl-β-methylcholine (methacholine, Sigma-Aldrich, Aston Manor, South Africa) (0, 5, 10, 20 and 40 mg/mL) for Balb/C or (0, 20, 40, 80 160 and 320 mg/mL) for C57BL/6. Differences in the dose-response curves were analysed by repeated-measures Two-way ANOVA with the Bonferroni post-test. Only mice with acceptable measurements for all doses (coefficient of determination >0.90) were included in the analysis.

Flow cytometry

Single-cell suspensions were prepared from lymph nodes in Roswell Park Memorial Institute (RPMI) media (Gibco, Paisley, United Kingdom) by passing them through 100μm strainer. To obtain single cell suspensions from lung tissues, a left lobe was digested for 1 hour at 37^{o}C in RPMI containing 13 mg/mL DNase I (Roche, Randburg, South Africa) and 50 U/mL collagenase IV (Gibco, Waltham, Massachusetts) and passed through 70μm strainer. Antibodies used in these experiments included, phycoerythrobilin (PE)- conjugated anti-Siglec-F (clone, E50-2440), anti-IL-5 (clone, TRFK5), anti-CD44 (clone, KM114), anti- T and B cell activation antigen (clone, GL7), anti-CD43 (clone, S7), FITC- conjugated anti-Ly6G (clone, 1A8), anti-IgD (clone, 11-

26C2a), IL-4 (clone, 11B11), anti-PD-1-(clone, 29F.1A12), PerCP Cy5.5- conjugated anti-Ly6C (clone, AL-21), -CD45.1 (clone, A20), anti-IL-17 (clone, TC11-18H10), anti-mouse alpha muscle actin (Abcam, ab8211-500), Allophycocyanin (APC)- conjugated anti-CD11c (clone, HL3), anti-CD5 (clone, 53-7.3), BV421 conjugated anti-CD11b (clone, M1/70), anti-CD62L (clone, MEL-14), anti-IgG1 (clone, A110-1), AlexaFlour 700- conjugated anti-CD3ε (clone, 145-2C11) -anti-IFN-γ (clone, XMG1.2), BV510-anti-CD4 (clone, RM4-5) and anti- B220 (clone, RA3-6B2), APC-Cy7-conjugated anti-CD19 (clone, 1D3) and anti-CD8 (clone, 53-6.7), BV786 conjugated anti-IgE (clone, R35-72) and anti-IL-33R (ST2) (clone, U29-93), biotin-conjugated anti-IgM (clone, AF-78), anti-CD95 (clone, Jo2), anti- CD249 (clone, BP-1) , anti-CD45 (clone, 30-F11) were purchased from BD Pharmingen (San Diego, CA). PE-Cynanine7 anti-F4/80 (clone, BM8), anti-IL-13 (clone, eBio13A), anti-CXCR5 (clone, L138D7), AlexaFlouro 700- conjugated anti-MHC II (clone, M5/114), Rabbit anti-BAIAP2L1 (Abcam, PA554000), Live/dead Fixable Yellow stain (Qdot605 dead cell exclusion dye) were purchased from eBiosciences. Biotin-labelled antibodies were detected by Texas Red conjugated PE (BD Biosciences). PE-Goat anti-Rabbit IgG (Abcam, ab72465) was used to detect Rabbit anti-BAIAP2L1. For staining, cells (1 x 10^6) were stained and washed in PBS, 3% FCS FACS buffer. For intracellular cytokine staining, cells were restimulated with phorbal myristate acetate (Sigma-Aldrich) (50 ng/mL), ionomycin (Sigma-Aldrich) (250ng/mL), and monensin (Sigma-Aldrich) (200mM in IMDM/10% FCS) for 5h at 37˚C then fixed in 2% PFA, permeabilised with Foxp3 transcriptional factor staining buffer kit (eBioscience) before intracellular staining with appropriate cytokine antibodies and acquisition through LSR Fortessa machine (BD Immunocytometry system, San Jose, CA, USA) and data was analysed using Flowjo software (Treestar, Ashland, OR, USA).

Histology

Left upper lung lobes was fixed in 4% formaldehyde/PBS and embedded in paraffin. Tissue sections were stained with periodic acid-Schiff for mucus secretion, and haematoxylin and eosin (H&E) stain for inflammation. Slides were scanned at 20x magnification on the virtual slide VS120 microscope (Olympus, Japan). Downstream processing of images was done through Image J (FIJI) for image extraction at series 15 and Ilastik software was used for mucus area quantification on whole lung sections. The data shown are representative of 1 experiment of 3 independent experiments (n = 5-7 mice per experiment).

Antibody and cytokine ELISAs

Antibody ELISAs were carried out as previously described[33] using 10 μg/ml HDM to coat for specific IgGs. Total IgE in serum was measured using anti-mouse IgE (BD Biosciences, 553413) to coat, mouse IgE (κ, anti-TNP, BD Biosciences, 557079) as standard and biotin anti-mouse IgE (BD Biosciences, 553419) as a secondary antibody.

For *in vitro* cytokine production analysis, single-cell suspensions were prepared from mediastinal lymph nodes of HDM-treated and littermate control mice. Cells ($2x10^5$ cells, in 200μL) were incubated for 5 days in RPMI/10% FCS (Delta Bioproducts, Kempton Park, South Africa) in 96-well plates. Cells were either stimulated with HDM (30μg/mL) or plate bound anti-CD3 (10μg/mL) and supernatants were collected after a 5-day incubation period. Concentrations of IL-4, IL-5 (BD Biosciences) and IL-13 (R&D Systems, Minneapolis, Minn), were measured using ELISA assays according to the manufacturer's protocol.

RNA Extraction

Small lung lobe was frozen in Qiazol (Qiagen, Germany) and stored at −80°C. Total RNA was isolated from the lysate using miRNeasy Mini kit (Qiagen, Germany) according to the manufacturer's instructions. RNA quantity and purity were measured using the ND-1000 NanoDrop spectrophotometer (ThermoScientific, DE, USA).

cDNA Synthesis and RT-qPCR

For *Muc5a* gene expression analysis, 100 ng total RNA was reverse transcribed into cDNA using Transcriptor First Strand cDNA Synthesis Kit (Roche, Germany) according to the manufacturer's instructions. Quantitative real-time PCR (RT-qPCR) was performed using LightCycler® 480 SYBR Green I Master (Roche, Germany) and *Muc5a* primers (IDT, CA, USA). Fold change in gene expression was calculated by the ΔΔCt method and normalized to ß-*actin* which was used as an internal control.

Whole lung RNA sequencing

Whole lung RNA was extracted using RNAeasy kit (Qiagen, Germany) according to the manufacturer's instructions. We used Agilent 2100 Bio analyzer (Agilent RNA 6000 Nano Kit) to do the total RNA sample QC: RNA concentration, RIN value,28S/18S and the fragment length distribution. The first step in the workflow involved purifying the poly-A containing mRNA molecules using poly-T oligo attached magnetic beads. Following purification, the mRNA was fragmented into small pieces using divalent cations under elevated temperature. The cleaved RNA fragments were copied into first strand cDNA using reverse transcriptase and random primers. This was followed by second strand cDNA synthesis using DNA Polymerase I and RNase H. These cDNA fragments had addition of a single 'A' base and subsequent ligation of the

adapter. The products were then purified and enriched with PCR amplification. PCR yields were quantified by Qubit and pooled samples together to make a single strand DNA circle (ssDNA circle), which gave the final library. DNA nanoballs (DNBs) were generated with the ssDNA circle by rolling circle replication (RCR) to enlarge the fluorescent signals at the sequencing process. The DNBs were loaded into the patterned nanoarrays and pair-end reads of 100 bp were read through on the DNBseq platform for the following data analysis study. For this step, the DNBseq platform combines the DNA nanoball-based nanoarrays and stepwise sequencing using Combinational Probe-Anchor Synthesis Sequencing Method.

Bioinformatics workflow

The ribosomal RNA (rRNA) was first removed using SortMeRNA. We then did the Fastq file quality control using Fastqc and multiqc software to assess the quality of the raw reads followed by adapter trimming using Trim galore. The reads were then aligned to the mouse reference genome (mm10_UCSC_20180903) using STAR aligner. The map read counts was then extracted using featurecounts. The gene differential analysis was conducted using the DEseq2. The genes with LFC >= 2 and adjusted p-value <= 0.05 was used to do the gene ontology over-representation analysis done using clusterProfiler[34] Bioconductor package. The Benjamini-Hochberg method was used for multiple test correction.

Human bronchial Airway Smooth Muscle cell culture

A healthy human bronchial smooth muscle cell line (BSMC, Lonza) was cultured in Smooth Muscle Growth Medium (Lonza) supplemented with Insulin (CC-4021D), human Fibroblastic Growth Factor-B (CC-4068D), Gentamicin sulfate-Amphotericin-

1000 (CC-4081D), 5% Foetal Bovine Serum (CC-4102D), human Epidermal Growth Factor (CC-4230D) (all purchased from Lonza) in a T25 flask (Lonza) until confluence. After two passages in the T75 flask, confluent cells were seeded at 1.6×10^5 BSMC cells onto 24-well trays and immediately transfected with CRISPR/Cas9 single guide RNAs.

CRISPR/Cas9 single guide RNA transfections

single guide RNAs targeting human *BAIAP2L1* (# CD.Cas9.CXVQ6494.AA); *ERDR1*, (# CD.Cas9.YFVV2490.AA); HPRT Negative Control (#Alt-R® CRISPR-Cas9crRNA) were purchased (IDT, CA, USA via WhiteScientific PTY LTD). Single guide RNA (1 μM) and Cas9 enzyme (1 μM) in Opti-MEM medium (Life Technologies™, Carlsbad, CA, USA) were transfected using Lipofectamine RNAi Max 1000 (Thermo Scientific) into BSMC cells ($1.6\ x10^5$) per well and either stimulated with Acetylcholine (10μM), recombinant human IL-13 (100 ng/mL), recombinant human TNF-α (10 ng/mL) or left unstimulated for 48 hours at 37°C, 5% CO_2 incubator. Gene deletion was confirmed by DNA extraction (Wizard Genomic DNA Purif. Kit, Promega) and PCR amplification of target genes using *BAIAP2L1* forward (GTCCCGGGGGCCCGA) and reverse (AAGCGCCCAAGAATGTGGGG) primers, and product run on a 1.2% agarose gel.

Cytotoxic detection Assay

To measure cytotoxicity after single guide RNA transfection, lactate dehydrogenase (LDH) was measured in supernatants collected at 48 hours post transfection using cytotoxicity detection kit ^{PLUS} Assay (CYTODET-RO, Roche) according to manufacturer's instructions and plates were read at 490 nm.

Single-cell force cytometry using Fluorescently Labelled Elastomeric Contractible Surface (FLECS) technology

BSMCs were seeded on Fibronectin-coated elastomeric micropatterns (Forcyte Biotechnologies #F2AX0G03Y, 50 microns, Alexa Fluor 488 - bound Fibrinogen, 24-well plate) at a concentration of 75,000 cells per well in Smooth muscle growth medium (SmGM) (Lonza) and left to adhere and spread for 90 minutes. Unattached cells were then removed and fresh SmGM medium supplemented with rhTNF-α (10 ng/mL)/rhIL-13 (100 ng/mL)/ACh (10μM) was added. BSMCs were stimulated for 3 hrs before being fixed in pre-warmed to 37^{o}C 4% PFA. Fixed samples were washed and then stained with ATTO-565 phalloidin (ATTO-TEC) and DAPI (Life Technologies) and imaged on a StellarVision microscope using Synthetic Aperture Optics technology (Optical Biosystems). All images were analyzed using FiJi software by measuring the length of each micropattern per condition after stimulation and subtracting the length of the unstimulated micropattern of the same condition.

Immunofluorescent

Left upper lung lobes were fixed in 4% formaldehyde/PBS and embedded in paraffin. Tissue sections (5 μm) were deparaffinised and hydrated in water before antigen retrieval in boiling 10 mM Citrate buffer (pH 6, pressure cooker for 2 mins). Tissue was incubated with Rabbit anti-BAIAP2L1 (Abcam, PA554000) in PBS-Tween (1:250, overnight, 4^{o}C) and FITC anti-mouse alpha muscle actin (Abcam, ab8211-500, 1:100, overnight, 4^{o}C). Tissues were washed with PBS-Tween before incubation with secondary antibody PE-Goat anti-Rabbit IgG (Abcam, ab72465) in PBS-Tween (1:500, RT in the dark for 30min). Tissues were washed with PBS-Tween before

mounting in DAPI mounting media (Thermofisher). Fluorescent images were captured at 60x magnification using LSM880 Airy Scan (Zeiss, UK).

Western blotting

Protein harvest: RIPA lysis buffer supplemented with protease inhibitors was added to the lung tissue. The whole-cell lysates were incubated on ice for 20 min and vortexed every 5 min for 60 seconds. Then, the lysate was centrifuged at 3000 rpm for 15 minutes at 4°C, and the supernatant was collected. Total protein concentrations were determined using the Pierce BCA Assay kit.

SDS-PAGE: 20 µg of each protein sample was mixed with Laemmli buffer and heated for 10 minutes at 100 °C. Equal amounts of protein samples were loaded into 5% acrylamide stacking gel and a 12% acrylamide separating gel along with 5 µL PageRulerTM Plus Prestained protein ladder (catalogue #: 26619, Thermo ScientificTM) and separated by electrophoresis at 100 V. Proteins were transferred onto nitrocellulose membranes (Bio-Rad) using the Bio-Rad Mini Trans-Blot® Cell according to the manufacturer's instructions.

After protein transfer, the nitrocellulose membranes were stained with Ponceau stain for approximately 1-3 minutes to visualize if the proteins had been transferred. Once the protein bands were identified, the membrane was washed with ddH_2O until 80% of the Ponceau staining is removed. The remaining 20% of the stain allowed the accurate segmentation of the membrane to separate high molecular weight proteins from low molecular weight proteins. The nitrocellulose membranes were blocked with 5 % (w/v) non-fat milk, 0.01% Tween-20 in TBST) on the shaker at room temperature

for one hour. The low and high molecular weight membranes proteins were incubated with respective primary antibodies (Rabbit anti-human BAIAP2L1, PA5-54000, Invitrogen) or (Goat anti-mouse GAPDH, sc 365062, Santa Cruz) overnight shaking in the 4°C cold room. Membranes were washed 4 times with 1xTBST in 15-minute intervals. Horseradish peroxidase (HRP) secondary antibodies were added to their respective membranes and incubated for one hour at room temperature, with shaking. subsequently, membranes were washed 3 times in 1xTBST in 15 minutes intervals. To visualise the protein bands on autoradiographic film (Santa Cruz Biotechnology®), Lumino Glo® substrate kit was added to each membrane. Briefly, the substrate luminol was oxidised by hydrogen peroxide in the presence of the catalyst HRP to yield a chemiluminescent product.

Plating of faecal pellets to confirm a reduction in bacterial colonies following antibiotic treatment.

The faecal pellet was collected from each individual mouse treated with antibiotics as well as control groups not treated with antibiotics. The faecal pellet was weighed and resuspended in sterile PBS at a concentration of 50 mg/mL. The sample was resuspended until homogenous, and 1/100 dilution was made in sterile PBS. 50μL of 1/100 dilutions was plated on tryptic soy agar plates and spread evenly across the plate before incubating at 37^{o}C for 16 hrs. Individual colonies were counted manually.

Statistical analysis

P-values were calculated in GraphPad Prism 6 (GraphPad Software, Inc) by using nonparametric Mann-Whitney Student's t-test or Two-way ANOVA with Bonferroni's post-test for multiple comparisons, and results are presented as standard error of the

401 mean (SEM) or mean of standard deviation (SD). Differences were considered
402 significant if P was <0.05.
403
404

RESULTS

IgM-deficient mice show profound airway hyperresponsiveness reduction when exposed to HDM.

We sensitised and challenged IgM-deficient ($IgM^{-/-}$) and wild-type Balb/c (WT) mice with HDM intratracheally (i.t.) and analysed AHR, lung infiltrates and cytokines (Fig. 1a, Supplementary Fig. 1a). We found moderately reduced resistance and elastance in $IgM^{-/-}$ sensitised with a high dose of HDM (100μg) compared to WT mice (Supplementary Fig. 1b). Similarly, we also observed a profound reduction in AHR in $IgM^{-/-}$ mice sensitised with a low dose of HDM (1μg) compared to WT (Fig. 1b). Interestingly, lung eosinophils were intact at both low dose (Fig. 1c) and high dose HDM (Supplementary Fig. 1d). We could also show that AHR reduction in $IgM^{-/-}$ mice was not allergen-specific, as we observed similar findings using ovalbumin (OVA) complexed to alum adjuvant (Supplementary Fig. 2a-b) and acute papain-induced allergic inflammation (Supplementary Fig. 2c-d). We observed similar finding of profound AHR reduction in $IgM^{-/-}$ mice in C57BL/6 background compared to WT mice (Supplementary Fig. 3a). These findings suggested that IgM-deficient mice have profound AHR reduction independent of allergen or mice background strain.

IgM-deficiency does not impact B cell subsets in primary and secondary organs, but class switching is impaired.

We also observed no significant changes between $IgM^{-/-}$ and WT mice in mucus production shown by *Muc5a* gene expression (Fig. 1d) or goblet cells in Balb/C (Supplementary Fig. 1f) and C57BL/6 mice challenged with HDM (Supplementary Fig. 3b). Accompanying reduction in AHR in $IgM^{-/-}$ mice was low titers of total IgE, HDM-specific IgE, and mediastinal lymph node (mLN) B cell surface expression of IgM and

IgG1 (Fig. 1e-f), owing to a lack of class switching. Interestingly, the numbers of lung B cells were normal (Fig. 1c and Supplementary Fig. 1c) and the frequencies of B cell subsets such as follicular, marginal zones and germinal centres (GCs) B cells were not affected by lack of IgM (Fig. 1g and Supplementary Fig. 1g). The lack in class switching in Balb/C mice was also consistent with what we found in $IgM^{-/-}$ mice in the C57BL/6 background (Supplementary Fig. 3c). This suggested a normal interaction between B and T cells in GCs, but lack of AID-dependent class switching, despite increased expression of IgD (Supplementary Fig. 4a) [35]. We checked for natural IgM and antigen-induced IgM in multiple tissues. B cells expressing IgD were increased in all tissues including mLNs, peritoneal cavity and spleen (Supplementary Fig. 4a-c) and pre-B cell subsets were normal in BM (Supplementary Fig. 4d) in the absence of IgM as previously reported [32].

T helper 2 cells are intact in the absence of IgM, and serum transfer can partially restore antibody function

To investigate whether the reduction in AHR was due to reduced Th2 cells and cytokines, we stimulated total mLN and lung cells with anti-CD3 for 5 days or with PMA/ionomycin for 5 hrs in the presence of monensin and measured secreted or intracellular IL-4 and IL-13 expression. We found no differences in CD4 T cells and T follicular helper cells (Fig. 2a) in mLN and in secreted or intracellular levels of IL-4 and IL-13 between $IgM^{-/-}$ and WT mice challenged with HDM in both mLN and lungs (Fig. 2b-c). To investigate what drives this reduced AHR in the absence of IgM between secreted antibodies or the IgM B cell receptor on the surface of B cells, we transferred serum from naïve WT mice into $IgM^{-/-}$ mice a day before sensitization, during sensitisation and a day before challenge with HDM allergen (Fig. 2d), as previously

455 described [36]. AHR in IgM$^{-/-}$ was still reduced compared to WT mice even after the
456 transfer of WT serum (Fig. 2e), but levels of total IgE, HDM-specific IgE and HDM-
457 specific IgG1 were increased and comparable to those found in WT mice (Fig. 2f and
458 Supplementary Fig. 5e). The redundant role of IgE was consistent with previous
459 studies where IgE nor its high-affinity receptor (FcεRI) were essential in AHR in an
460 HDM or OVA models [30]. The lack of functional role of serum-transferred IgE was
461 consistent with earlier findings on *H. polygyrus* transfer of immune serum where IgE
462 was found not to be essential in protection against *H. polygyrus* re-infection [36]. We
463 also tried to restore IgM function through adoptive reconstitution with congenic CD45.1
464 BM or sorted B cells into IgM$^{-/-}$ mice (Supplementary Fig. 5a). This approach did not
465 replenish IgM B cells to levels observed in WT mice and as a result did not restore
466 AHR, total IgE and IgM in these mice (Supplementary Fig. 5b-c). To understand why
467 we could not reconstitute IgM, we checked for transferred congenic B cells in different
468 organs after reconstitution with WT BM in IgM$^{-/-}$ mice and found some engraftment in
469 BM and spleen, but poor engraftment to lung and mLNs which may partially explain
470 our inability to restore AHR in IgM$^{-/-}$ mice challenged with HDM (Supplementary Fig.
471 5d).
472
473 IgM is known to play key role in shaping gut microbiota and its diversity can be shaped
474 by gut commensals [16,37]. To understand whether microbiota could influence AHR in
475 IgM-deficient mice, we treated WT and IgM$^{-/-}$ with an antibiotic cocktail 3x per week for
476 2 weeks (Supplementary Fig. 6a). We confirmed the reduction of bacteria in the faecal
477 pellet after 2 weeks of antibiotic treatment (Supplementary Fig. 6a). We then
478 sensitised and challenged these mice with HDM and measure AHR (Supplementary
479 Fig. 6b). We observed increased resistance and elastance in WT mice compared to

IgM$^{-/-}$ mice and pre-treatment with antibiotics did not influence AHR (Supplementary Fig. 6b). Treatment with antibiotics did increase total IgE, HDM-specific IgE and IgG1 in WT mice as expected[38], but had no impact on IgM-deficient mice (Supplementary Fig. 6c), suggesting that overall antibiotics did not influence AHR.

RNA sequencing reveals enrichment of genes associated with skeletal muscle contraction and actin re-arrangement.

Because we had found no other changes in asthmatic allergic features between WT and IgM$^{-/-}$, except for profoundly reduced AHR, we resorted to RNA sequencing to see if there were lung-specific factors that influenced AHR regulation in IgM-deficient mice. Principal component analysis (PCA) depicted distinct global transcriptional changes with PC1 and PC2 explaining most of the variation (Fig. 3a). We found a smaller variation in gene expression between WT and IgM$^{-/-}$ in both HDM-challenged and PBS control mice (Fig. 3b). We could mainly detect downregulation of genes such as brain-specific angiogenesis inhibitor 1-associated protein 2-like protein 1 (*Baiap2l1*), erythroid differentiation regulatory factor 1 (*Erdr1*), chemokines such as *Ccl8*, *Ccl9*, *Ccl17* and *Ccl22* in IgM$^{-/-}$ mice challenged with HDM (Fig. 3c-d). Interestingly, *Baiap2l1* and *Erdr1* were also downregulated in IgM$^{-/-}$ saline-treated control mice, suggesting an inflammation-independent effect (Fig. 3c and e). We also found the presence of the J-chain coding gene in WT mice which was absent in IgM$^{-/-}$ mice, confirming a deletion in genes associated with holding IgM monomers together and thus IgM [39] (Fig. 3e). Gene set enrichment analyses (GSEA) confirmed that the genes contributing to changes in AHR between WT and IgM$^{-/-}$ were associated with muscle system processes and skeletal muscle contraction (Fig. 3f). There was also an over-representation of gene ratios associated with skeletal muscle development,

differentiation and contraction, and suppression of genes associated with chemotaxis and plasma membrane-bounded cell projection (Supplementary Fig. 7).

***BAIAP2L1* is expressed in lung cells in contact with airway smooth muscle cells.** We decided to focus on *Baiap2l1* also known as Inverse-bin-amphiphysin-Rvs (I-BAR)-domain-containing protein insulin receptor tyrosine kinase substrate (IRTKS), which has been shown to promote actin polymerisation and microvilli length in the intestinal epithelial cells [40]. We first verified whether BAIAP2L1 was also downregulated at the protein level in IgM-deficient mouse lungs challenged with HDM (Fig. 4a). We found lower expression levels of BAIAP2L1 in IgM-deficient mice compared to WT mice challenged with HDM by western blotting, although this was not significant (Fig. 4a). Human Protein Atlas search suggested that BAIAP2L1 is expressed by multiple cell types including fibroblasts, skeletal muscle, smooth muscle and macrophages [41]. We then investigated by immunofluorescence which cell types within the lung could be expressing BAIAP2L1 (Fig. 4b). We found BAIAP2L1 to be closely expressed within structural cells in close contact to smooth muscle cells (less than 10μm), a cell type known to be essential in bronchoconstriction. Airway smooth muscle together with the extracellular matrix contributes to smooth muscle hypertrophy which causes the narrowing of the airways. These cells by histology appear to be separated due to fixation methods but are mashed together, especially during the remodelling of the airways [42]. IgM deficiency did not impact this expression in cells in close contact with smooth muscle (Fig. 4b). Because both western blot and immunofluorescent were inconclusive, we also verified the expression of BAIAP2L1 via flow cytometry (gating in Supplementary Fig. 8a) and found it to be expressed mainly by alpha-smooth muscle cells and increased in expression in HDM treated mice

compared to PBS control mice (Fig. 4c). Furthermore, we showed a reduction in BAIAP2L1 expression amongst alpha-smooth muscle cells but not other cells (CD45 positive or alpha-smooth muscle negative cells, Supplementary Fig. 8b) in IgM-deficient mice compared to WT mice treated with HDM, although this did not reach significance (Fig. 4c). Overall, this data suggested that BAIAP2L1 is reduced at RNA and protein level and likely influenced the reduction of AHR in IgM-deficient mice. This was consistent with gene set enrichment in our RNA seq data where there was a dominance of genes associated with muscle contraction which regulates AHR.

CRISPR-Cas9 deletion of *BAIAP2L1* leads to reduced airway smooth muscle contraction at a single cell.

To understand how *Baiap2l1*, one of the genes downregulated in IgM-deficient mice, could influence AHR, we resorted to an *in vitro* model that allowed us to measure contraction using fluorescently labelled elastomeric contractible surface (FLECS) technology [43] (Fig. 5a). We opted for airway smooth muscle as it has been shown to contribute to the narrowing of the airway during an allergic attack and together with neighbouring cells such as extracellular matrix and immune cells are critical in hypertrophy [42]. We chose the human bronchial smooth muscle cell (BSMCs) line as *BAIAP2L1* is expressed in structural cells including muscle and epithelial cells, and actin together with myosin is essential in muscle contraction [41]. To this end, we used CRISPR-Cas9 technology to knock down *BAIAP2L1* in BSMCs (Supplementary Fig. 9a-b). We also included ERDR1 as one of the genes that were also downregulated in IgM-deficient mice. BSMCs (160 000/well) were stimulated with 10μM acetylcholine (ACh), 10 ng/mL of human TNF-α and 100 ng/mL IL-13, followed by transfection with ribonucleoprotein (RNP) complexes containing single guide RNA targeting *BAIAP2L1*

555 and Cas9 for 48h (Fig. 5b). Transfected cells were seeded onto elastomeric patterns,
556 stimulated with the same stimulants for 3h and fixed in 4% paraformaldehyde, followed
557 by staining with DAPI and Phalloidin before imaging on Stellarvision microscope and
558 quantification (Fig. 5a). We validated the deletion of *BAIAP2L1* by PCR and showed
559 reduced expression of *BAIAP2L1* in ACh and TNF-α stimulated cells transfected with
560 *BAIAP2L1* sgRNA when compared to scramble sgRNA (Supplementary Fig. 9c, line
561 3 and 4 compared to line 5 and 6). We also detected low expression of BAIAP2L1 in
562 unstimulated sgRNA scramble and sgRNA *BAIAP2L1* transfected cells
563 (Supplementary Fig. 9c, lines 1 and 2). Transfections with sgRNA did not impact cell
564 viability (Supplementary Fig. 9d). As expected, BSMCs displayed a higher level of
565 contraction in TNF-α or IL-13 stimulated cells compared to unstimulated cells (Fig. 5b-
566 d). In BSMCs transfected with sgRNA-*BAIAP2L1* and -*ERDR1*, we saw a significant
567 reduction in contraction levels in TNF-α stimulated cells when compared to scramble
568 sgRNA transfected and stimulated cells (Fig. 5b, c). We saw no differences in
569 contraction between scramble sgRNA and sgRNA-*BAIAP2L1* and -*ERDR1* stimulated
570 with IL-13 (Fig. 5d).
571
572 ***BAIAP2L1* deletion but not *ERDR1* is essential in acetylcholine-induced smooth**
573 **muscle contraction.**
574 Contraction of the ASM is central to AHR as it controls airway diameter and airflow
575 which can increase resistance [20]. Airway smooth muscle contractility is induced when
576 extracellular factors such as ACh bind through muscarinic 3 acetylcholine receptor
577 (m_3AChR), activating a signalling cascade leading to calcium accumulation and
578 contraction [44]. We transfected BSMCs with sgRNA-*BAIAP2L1*, -*ERDR1* or scrambled
579 and stimulated cells with 10 μM ACh (Fig. 6a). We saw a significant reduction in BSMC

contraction transfected with sgRNA-*BAIAP2L1* when compared to scramble sgRNA transfected and ACh stimulated (Fig. 6b-c). We saw no significant differences in BSMC contraction between sgRNA-*ERDR1* transfected and scramble sgRNA transfected and ACh stimulated cells (Fig. 6b-c). Taken together, this data indicates that *BAIAP2L1* a gene that was downregulated in IgM-deficient mice has a stimulant-specific role in inducing airway contraction of bronchial smooth muscle cells during asthma.

DISCUSSION

Here, we described an unexpected function of IgM in the regulation of bronchoconstriction. We show by RNA sequencing that in the lung tissue of IgM-deficient mice, there is a reduction in genes (*Baiap2l1* and *Erdr1*) associated with actin cytoskeleton and re-arrangement, a key factor in smooth muscle contraction and AHR. We used single-cell force cytometry and CRISPR-Cas9 technology to validate these genes in the human BSM cell line and show as a proof of concept that deletion of *BAIAP2L1* reduced muscle contraction in a stimulant-specific manner.

B cells play a complex role in allergic asthma, earlier studies using B cell-deficient mice showed a redundant role of B cells in OVA-induced allergic airway inflammation and airway hyperreactivity [27–29]. We and others have recently shown using a more complex allergen HDM relevant to human asthma that antigen load is crucial in B cell function [22–24]. We explored these possibilities in the context of IgM deficiency and observed a profound reduction in AHR. This was in complete contrast to what has been observed in B cell-deficient mice and in IgE or FcεRI-deficient mice [23,24,30]. We also found a similar reduction in AHR at higher doses of HDM, albeit less pronounced.

Reduction in AHR was not only specific to HDM, but we also found reduced AHR in IgM-deficient mice sensitised with OVA complexed to alum and challenged with OVA, although less pronounced. AHR reduction in IgM-deficient mice was also seen in the acute papain model which only activates innate responses including innate lymphoid cells [45]. Interestingly, this reduction in AHR was not associated with reduced allergic airway inflammation including eosinophilia, mucus production or Th2 cells in all models tested, which was unexpected considering these features are key in AHR. B cell-deficient mice show a reduction in eosinophilia and antigen-specific Th2 cells at low doses of HDM, which leads to reduced AHR [24]. Similar findings are observed in mice lacking IL-4Rα specifically in B cells when challenged with HDM [22].

IgM deficiency did not impact B cell development in primary and secondary lymphoid tissues and accumulation of follicular and germinal centre B cells. Interestingly, there was a lack of class switching to IgG1 and IgE isotypes despite increased expression of IgD. The lack of class switching to IgG1 and IgE contrasts with earlier reports, which suggested that IgD can largely replace IgM for class switching to other isotypes, resulting in delayed neutralising IgG1 against vesicular stomatitis virus (VSV) [32,46]. To get a better understanding of which IgM function was responsible for AHR, we showed that the transfer of naïve wild-type mice serum to IgM-deficient mice could restore IgE production and HDM-specific IgE and IgG1. This is consistent with what has been observed in the context of influenza viral infections, where the transfer of purified or serum IgM into B cell-deficient mice restored IgM-induced viral neutralisation [47]. We believe that naïve sera transferred to IgM-deficient mice were able to bind to the surface of B cells via IgM receptors (FcμR / Fcα/μR), which are still present on IgM-deficient B cells, and this signalling is sufficient to facilitate Class Switch

Recombination (CSR). This was also confirmed by the ability of B cells to reach germinal centres in IgM-deficient mice during HDM exposure. Our $IgM^{-/-}$ mouse lacks both membrane-bound and secreted IgM, and transferred serum contains at least secreted IgM which can bind to B cell surfaces. Of course, we can't rule out that transferred sera from WT mice also contains some IgG1 which can facilitate class switching to IgE when transferred to IgM-deficient mice. Despite the ability of wild-type serum to restore IgE, it was not enough to restore AHR, which may be due to the difficulties in restoring IgM to normal levels (200-800 μg). Our findings on the redundant role of IgE were consistent with previous studies where IgE nor its high-affinity receptor (FcεRI) were essential in AHR in an HDM or OVA model [30]. The lack of functional role of serum-transferred IgE was consistent with earlier findings on *H. polygyrus* transfer of immune serum where IgE was found not to be essential in protection against *H. polygyrus* re-infection [36]. Our efforts to adoptively transfer wild-type bone marrow or sorted B cells into IgM-deficient mice were also largely unsuccessful partly due to poor engraftment of wild-type B cells into secondary lymphoid tissues. Natural secreted IgM is mainly produced by B1 cells in the peritoneal cavity, and it is likely that any transfer of B cells via bone marrow transfer would not be sufficient to restore soluble levels of IgM[3,10].

B cell isotype IgD has been shown to promote Th2 cells and OVA-, papain- and NP-specific humoral responses specifically IgG1 and IgE through basophil activation [31]. IgD has also been shown to inhibit IgE-mediated basophil activation through downregulation of genes associated with cytoskeleton organisation such as signal transducers phosphoinositide-3 kinase, RAS, and RHO [31]. Our RNA sequencing data showed downregulation of *Baiap2l1* and *Erdr1* in IgM-deficient mice, genes which

655 have been shown to associate with actin cytoskeleton and re-arrangement, [40,41,48].
656 Contraction of the ASM is central to AHR as it controls airway diameter and airflow
657 which can increase resistance [49]. ASM activated by cytokines such as IL-13 or TNF-α
658 or bronchoconstrictor ACh induces cytosolic calcium accumulation [49,50]. Ca^{2+} release
659 results in a cascade of events that involves kinases and phosphorylation of key
660 molecules such as actin and myosin involved in smooth muscle contraction [44]. Gene
661 set enrichment analysis suggested that genes downregulated in IgM-deficient mice
662 were involved in processes such as muscle contraction, muscle twitching, skeletal
663 muscle movement. As a proof of concept we validated the involvement of *BAIAP2L1*
664 in bronchial smooth muscle contraction using a high throughput method that allows us
665 to measure contraction of 1000s of single cells [43]. When we deleted *BAIAP2L1* using
666 CRISPR-Cas9, we showed that deletion of *BAIAP2L1* in BSMCs reduced smooth
667 muscle contraction when stimulated with TNF-α and ACh, but not IL-13. Deletion of
668 ERDR1 had minor impact on muscle contraction across different stimulants
669 suggesting a stimulant and gene-specific role. IRTKS/BAIAP2L1 has been shown to
670 regulate microvilli elongation by forming a complex with actin-regulating protein EPS8
671 [40]. In this setting IRTKS elongate microvilli via distinct mechanisms that require
672 functional WH2 and SH3 domains, which binds EPS8, an F-actin capping and bundling
673 protein [40]. We have not fully dissected how *BAIAP2L1* could be regulated by IgM, but
674 it is clear that through its actions to regulate actin bundling, it is involved in muscle
675 contraction which requires actin and myosin head interaction (summarised in Fig. 7).
676
677 We speculate that IgM can directly activate smooth muscle cells by binding a number
678 of its surface receptors including FcμR, Fcα/μR and pIgR [51–53]. IgM binds to FcμR
679 strictly, but shares Fcα/μR and pIgR with IgA [5,51,53]. Both Fcα/μR and pIgR can be

680 expressed by non-structural cells at mucosal sites [53,54]. We would not rule out that the
681 mechanisms of muscle contraction might be through one of these IgM receptors,
682 especially the ones expressed on smooth muscle cells[53,54]. Certainly, our future
683 studies will be directed towards characterizing the mechanism by which IgM potentially
684 activates the smooth muscle.
685
686 We believe these findings report for the first time an independent function of IgM from
687 its natural class switching and non-specific binding to microbial components. We
688 believe that IgM function in regulating ASM may be indirect through other unknown
689 factors but does not involve microbiota as treatment of mice with a mixture of
690 antibiotics did not restore AHR. Early vaccination with bacterial species, such as group
691 *A streptococcus* containing GlcNAc or β-1,3-glucans can protect adult mice against *A.*
692 *fumigatus*-induced allergic asthma [55]. This is mainly through conserved germline-
693 encoded IgM antibodies, which have broad specificities to common allergens
694 containing GlcNAc moieties such as Dermatophytes [8,56]. Together these findings
695 demonstrate for the first time an important function of IgM in regulating airway
696 hyperresponsiveness independent of the presence of T helper 2 allergic inflammation.
697 These findings have implications for future treatment of allergic asthma through
698 bronchodilators.
699
700 **Competing interests**
701 The authors declare that they have no competing interests.
702
703
704

Acknowledgements

We thank the UCT Research Animal Facility for maintaining mice, and Munadia Ansari for genotyping mice. We are grateful to Lizette Fick and Raygaana Jacobs for their excellent histology services and for confocal microscopy core facilities. We are grateful to Ronnie Dreyer for the excellent cell sorting and Flow Cytometry Core Facility. We thank FlowJo for proving free service to Africa.

Author contributions

Conceived and supervised study: SH FB. Performed the experiments: SH AFS JK KJ NM MS AN FM HN WM. Analysed the data: SH AFS KJ JO NM HN FM. Wrote the paper: SH FB. All authors discussed the results and commented on the manuscript.

Funding statement

This work was supported by ICGEB, Cape Town Component, Medical Research Council (MRC) South Africa as well as support by the South African National Research Foundation (NRF) Research Chair initiative (SARChi) and Wellcome Trust CIDRI-Africa (203135Z/16/Z) to FB. SH is supported by NRF Thuthuka Grant (117721), NRF Competitive Support for Unrated Researcher (138072), MRC South Africa under Self-initiated grant. NM was supported by the South African MRC PhD Fellowship. AN was supported by NRF MSc Scholarship. This research was funded in whole, or in part, by the Wellcome Trust [Grant number 203135Z/16/Z]. For the purpose of open access, the author has applied a CC BY public copyright licence to any Author Accepted Manuscript version arising from this submission.

References

1. Akula, S., Mohammadamin, S. & Hellman, L. Fc Receptors for Immunoglobulins and Their Appearance during Vertebrate Evolution. *PLoS One* **9**, e96903 (2014).
2. Blandino, R. & Baumgarth, N. Secreted IgM: New tricks for an old molecule. *J Leukoc Biol* **106**, 1021–1034 (2019).
3. Baumgarth, N. *et al.* B-1 and B-2 Cell–Derived Immunoglobulin M Antibodies Are Nonredundant Components of the Protective Response to Influenza Virus Infection. *Journal of Experimental Medicine* **192**, 271–280 (2000).
4. Ehrenstein, M. R. & Notley, C. A. The importance of natural IgM: scavenger, protector and regulator. *Nat Rev Immunol* **10**, 778–786 (2010).
5. Michaud, E., Mastrandrea, C., Rochereau, N. & Paul, S. Human Secretory IgM: An Elusive Player in Mucosal Immunity. *Trends Immunol* **41**, 141–156 (2020).
6. Quartier, P., Potter, P. K., Ehrenstein, M. R., Walport, M. J. & Botto, M. Predominant role of IgM-dependent activation of the classical pathway in the clearance of dying cells by murine bone marrow-derived macrophages in vitro. *Eur J Immunol* **35**, 252–260 (2005).
7. Wesemann, D. R. *et al.* Microbial colonization influences early B-lineage development in the gut lamina propria. *Nature* **501**, 112–115 (2013).
8. New, J. S. *et al.* Neonatal Exposure to Commensal-Bacteria-Derived Antigens Directs Polysaccharide-Specific B-1 B Cell Repertoire Development. *Immunity* **53**, 172-186.e6 (2020).
9. Kawahara, T., Ohdan, H., Zhao, G., Yang, Y.-G. & Sykes, M. Peritoneal Cavity B Cells Are Precursors of Splenic IgM Natural Antibody-Producing Cells. *The Journal of Immunology* **171**, 5406 LP – 5414 (2003).
10. Nguyen, T. T. T., Graf, B. A., Randall, T. D. & Baumgarth, N. sIgM–FcμR Interactions Regulate Early B Cell Activation and Plasma Cell Development after Influenza Virus Infection. *The Journal of Immunology* **199**, 1635 LP – 1646 (2017).
11. Jones, K., Savulescu, A. F., Brombacher, F. & Hadebe, S. Immunoglobulin M in Health and Diseases: How Far Have We Come and What Next? . *Frontiers in Immunology* vol. 11 2858 Preprint at (2020).
12. Yilmaz, B. *et al.* Gut Microbiota Elicits a Protective Immune Response against Malaria Transmission. *Cell* **159**, 1277–1289 (2014).
13. Krishnamurty, A. T. *et al.* Somatically Hypermutated Plasmodium-Specific IgM+ Memory B Cells Are Rapid, Plastic, Early Responders upon Malaria Rechallenge. *Immunity* **45**, 402–414 (2016).
14. Rapaka, R. R. *et al.* Conserved natural IgM antibodies mediate innate and adaptive immunity against the opportunistic fungus Pneumocystis murina. *Journal of Experimental Medicine* **207**, 2907–2919 (2010).
15. Subramaniam, K. S. *et al.* The absence of serum IgM enhances the susceptibility of mice to pulmonary challenge with Cryptococcus neoformans. *J Immunol* **184**, 5755–5767 (2010).
16. Magri, G. *et al.* Human Secretory IgM Emerges from Plasma Cells Clonally Related to Gut Memory B Cells and Targets Highly Diverse Commensals. *Immunity* **47**, 118-134.e8 (2017).

17. Weber, G. F. *et al.* Pleural innate response activator B cells protect against pneumonia via a GM-CSF-IgM axis. *Journal of Experimental Medicine* **211**, 1243–1256 (2014).
18. del Barrio, L. *et al.* Production of Anti-LPS IgM by B1a B Cells Depends on IL-1β and Is Protective against Lung Infection with Francisella tularensis LVS. *PLoS Pathog* **11**, e1004706 (2015).
19. Goldstein, M. F. *et al.* Selective IgM immunodeficiency: retrospective analysis of 36 adult patients with review of the literature. *Annals of Allergy, Asthma & Immunology* **97**, 717–730 (2006).
20. Lambrecht, B. N. & Hammad, H. The immunology of asthma. *Nat Immunol* **16**, 45–56 (2014).
21. Mandler, R., Finkelman, F. D., Levine, A. D. & Snapper, C. M. IL-4 induction of IgE class switching by lipopolysaccharide-activated murine B cells occurs predominantly through sequential switching. *The Journal of Immunology* **150**, 407 LP – 418 (1993).
22. Hadebe, S. *et al.* Deletion of IL-4Ra signaling on B cells limits hyperresponsiveness depending on antigen load. *Journal of Allergy and Clinical Immunology* **148**, 99-109.e5 (2021).
23. Habener, A. *et al.* Regulatory B cells control airway hyperreactivity and lung remodeling in a murine asthma model. *Journal of Allergy and Clinical Immunology* **147**, 2281-2294.e7 (2021).
24. Dullaers, M. *et al.* House dust mite–driven asthma and allergen-specific T cells depend on B cells when the amount of inhaled allergen is limiting. *Journal of Allergy and Clinical Immunology* **140**, 76-88.e7 (2017).
25. Ballesteros-Tato, A. *et al.* T Follicular Helper Cell Plasticity Shapes Pathogenic T Helper 2 Cell-Mediated Immunity to Inhaled House Dust Mite. *Immunity* **44**, 259–273 (2016).
26. Wypych, T. P., Marzi, R., Wu, G. F. & Lanzavecchia, A. Role of B cells in T H cell responses in a mouse model of asthma. *Journal of Allergy and Clinical Immunology* **141**, 1395–1410 (2020).
27. MacLean, J. A., Sauty, A., Luster, A. D., Drazen, J. M. & De Sanctis, G. T. Antigen-induced airway hyperresponsiveness, pulmonary eosinophilia, and chemokine expression in B cell-deficient mice. *Am J Respir Cell Mol Biol* **20**, 379–387 (1999).
28. Hamelmann, E. *et al.* Development of Eosinophilic Airway Inflammation and Airway Hyperresponsiveness Requires Interleukin-5 but Not Immunoglobulin E or B Lymphocytes. *Am J Respir Cell Mol Biol* **21**, 480–489 (1999).
29. Korsgren, M., ält, J. S. E., Korsgren, O., Sundler, F. & Persson, C. G. A. Allergic Eosinophil-rich Inflammation Develops in Lungs and Airways of B Cell–deficient Mice. *Journal of Experimental Medicine* **185**, 885–892 (1997).
30. McKnight, C. G., Jude, J. A., Zhu, Z., Panettieri, R. A. & Finkelman, F. D. House Dust Mite–Induced Allergic Airway Disease Is Independent of IgE and FcεRIα. *Am J Respir Cell Mol Biol* **57**, 674–682 (2017).
31. Shan, M. *et al.* Secreted IgD Amplifies Humoral T Helper 2 Cell Responses by Binding Basophils via Galectin-9 and CD44. *Immunity* **49**, 709-724.e8 (2018).
32. Lutz, C. *et al.* IgD can largely substitute for loss of IgM function in B cells. *Nature* **393**, 797–801 (1998).
33. Kirstein, F., Nieuwenhuizen, N. E., Jayakumar, J., Horsnell, W. G. C. & Brombacher, F. Role of IL-4 receptor α–positive CD4+ T cells in chronic airway hyperresponsiveness. *Journal of Allergy and Clinical Immunology* (2015) doi:10.1016/j.jaci.2015.10.036.

34. Wu, T. *et al.* clusterProfiler 4.0: A universal enrichment tool for interpreting omics data. *The Innovation* **2**, (2021).
35. Muramatsu, M. *et al.* Class Switch Recombination and Hypermutation Require Activation-Induced Cytidine Deaminase (AID), a Potential RNA Editing Enzyme. *Cell* **102**, 553–563 (2000).
36. Wojciechowski, W. *et al.* Cytokine-Producing Effector B Cells Regulate Type 2 Immunity to H. polygyrus. *Immunity* **30**, 421–433 (2009).
37. Smith, F. L. *et al.* B-1 plasma cells require non-cognate CD4 T cell help to generate a unique repertoire of natural IgM. *Journal of Experimental Medicine* **220**, e20220195 (2023).
38. Trompette, A. *et al.* Gut microbiota metabolism of dietary fiber influences allergic airway disease and hematopoiesis. *Nat Med* **20**, 159–166 (2014).
39. Norderhaug, I. N., Johansen, F.-E., Krajči, P. & Brandtzaeg, P. Domain deletions in the human polymeric Ig receptor disclose differences between its dimeric IgA and pentameric IgM interaction. *Eur J Immunol* **29**, 3401–3409 (1999).
40. Postema, M. M., Grega-Larson, N. E., Neininger, A. C. & Tyska, M. J. IRTKS (BAIAP2L1) Elongates Epithelial Microvilli Using EPS8-Dependent and Independent Mechanisms. *Current Biology* **28**, 2876-2888.e4 (2018).
41. Abo, H. *et al.* Erythroid differentiation regulator-1 induced by microbiota in early life drives intestinal stem cell proliferation and regeneration. *Nat Commun* **11**, 1–12 (2020).
42. James, A. L. *et al.* Airway Smooth Muscle Hypertrophy and Hyperplasia in Asthma. *Am J Respir Crit Care Med* **185**, 1058–1064 (2012).
43. Pushkarsky, I. *et al.* Elastomeric sensor surfaces for high-Throughput single-cell force cytometry. *Nat Biomed Eng* **2**, 124–137 (2018).
44. Ouedraogo, N. & Roux, E. Pulmonary & Respiratory Medicine Physiology of Airway Smooth Muscle Contraction : An Overview. *J Pulm Respir Med* **4**, 1–6 (2014).
45. Darby, M. *et al.* ILC3-derived acetylcholine promotes protease-driven allergic lung pathology. *Journal of Allergy and Clinical Immunology* **147**, 1513-1516.e4 (2021).
46. Ochsenbein, A. F. *et al.* Control of Early Viral and Bacterial Distribution and Disease by Natural Antibodies. *Science (1979)* **286**, 2156 LP – 2159 (1999).
47. Jayasekera, J. P., Moseman, E. A. & Carroll, M. C. Natural Antibody and Complement Mediate Neutralization of Influenza Virus in the Absence of Prior Immunity. *J Virol* **81**, 3487 LP – 3494 (2007).
48. Houh, Y. K., Kim, K. E., Park, H. J. & Cho, D. Roles of erythroid differentiation regulator 1 (Erdr1) on inflammatory skin diseases. *Int J Mol Sci* **17**, 1–10 (2016).
49. Perkins, C. *et al.* Selective stimulation of IL-4 receptor on smooth muscle induces airway hyperresponsiveness in mice. *J Exp Med* **208**, 853–867 (2011).
50. Moulton, B. C. & Fryer, A. D. Muscarinic receptor antagonists, from folklore to pharmacology; finding drugs that actually work in asthma and COPD. *Br J Pharmacol* **163**, 44–52 (2011).
51. Nguyen, T. T. T. *et al.* The IgM receptor FcμR limits tonic BCR signaling by regulating expression of the IgM BCR. *Nat Immunol* **18**, 321–333 (2017).
52. Shibuya, A. *et al.* Fcα/μ receptor mediates endocytosis of IgM-coated microbes. *Nat Immunol* **1**, 441–446 (2000).
53. Liu, J. *et al.* Role of the IgM Fc Receptor in Immunity and Tolerance. *Front Immunol* **10**, (2019).

54. Kim, M.-S. *et al.* A draft map of the human proteome. *Nature* **509**, 575–581 (2014).
55. Kin, N. W., Stefanov, E. K., Dizon, B. L. P. & Kearney, J. F. Antibodies Generated against Conserved Antigens Expressed by Bacteria and Allergen-Bearing Fungi Suppress Airway Disease. *The Journal of Immunology* **189**, 2246 LP – 2256 (2012).
56. Kearney, J. F., Patel, P., Stefanov, E. K. & King, R. G. Natural Antibody Repertoires: Development and Functional Role in Inhibiting Allergic Airway Disease. *Annu Rev Immunol* **33**, 475–504 (2015).

FIGURE LEGENDS

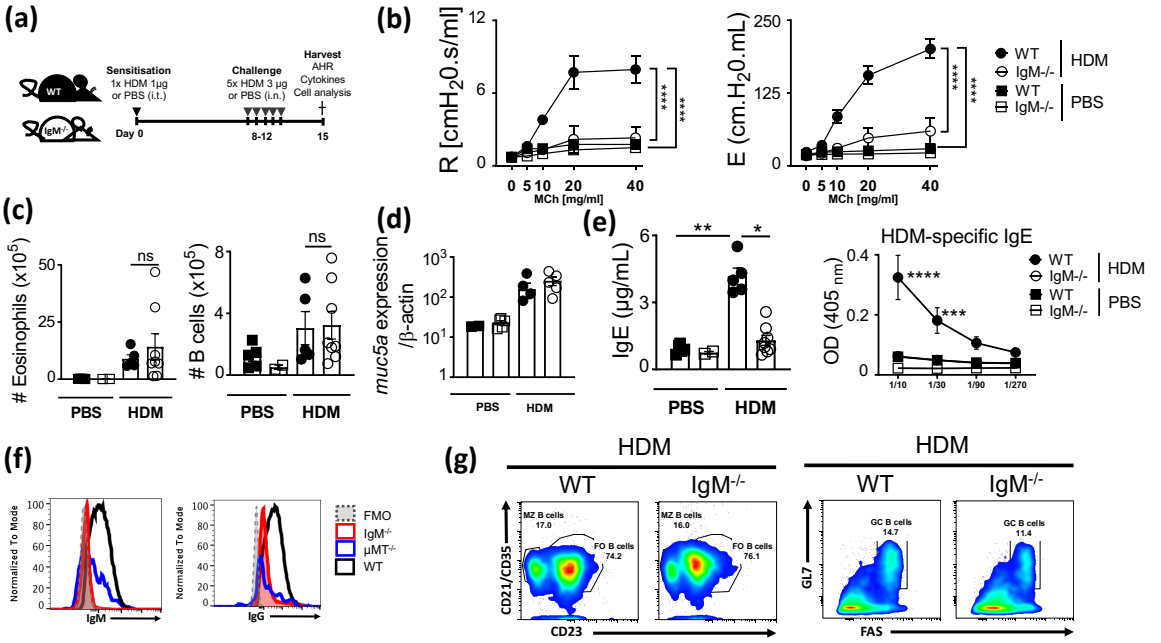

Figure 1

Fig. 1 IgM-deficiency leads to reduced airway hyperresponsiveness and class switching to IgE in HDM-induced asthma.

a Schematic diagram showing sensitisation and challenge protocol where mice ($IgM^{-/-}$) and wild type littermate control (WT) were sensitised with HDM 1 µg intra-tracheally on days 0 and challenged with HDM 3 µg on days 8-12. Analysis was done on day 15.

b Airway resistance and elastance were measured with increasing doses of acetyl methacholine (0 -40 mg/mL).

c Total lung eosinophil numbers ($live^{+}Siglec\text{-}F^{+}CD11c^{-}$) and B cells ($live^{+}B220^{+}CD19^{+}MHCII^{+}$) were stained and analysed by Flow cytometry and enumerated from % of live cells.

d *Muc5a* gene expression in whole lung tissue.

e Total IgE and HDM-specific IgE in serum.

f IgG1 and IgM surface expression in mediastinal lymph node B cells of WT, $IgM^{-/-}$ and $\mu MT^{-/-}$ mice.

g Marginal Zone ($live^+B220^+CD19^+MHCII^+CD21/CD35^+CD23^-$), follicular ($live^+B220^+CD19^+MHCII^+CD23^+CD21/CD35^+$) and Germinal Centre ($live^+B220^+CD19^+MHCII^+GL7^+FAS^+$) B cells in the mediastinal lymph node of WT and $IgM^{-/-}$ mice challenged with HDM.

Shown is mean ± SEM from two pooled experiments (n=7 - 10). Significant differences between groups were performed by Student *t*-test (Mann-Whitney) (c, d, e) or by Two-Way ANOVA with Benforroni post-test (b) and are described as: **p*<0.05, ***p*<0.01, ****p*<0.001, *****p*<0.0001.

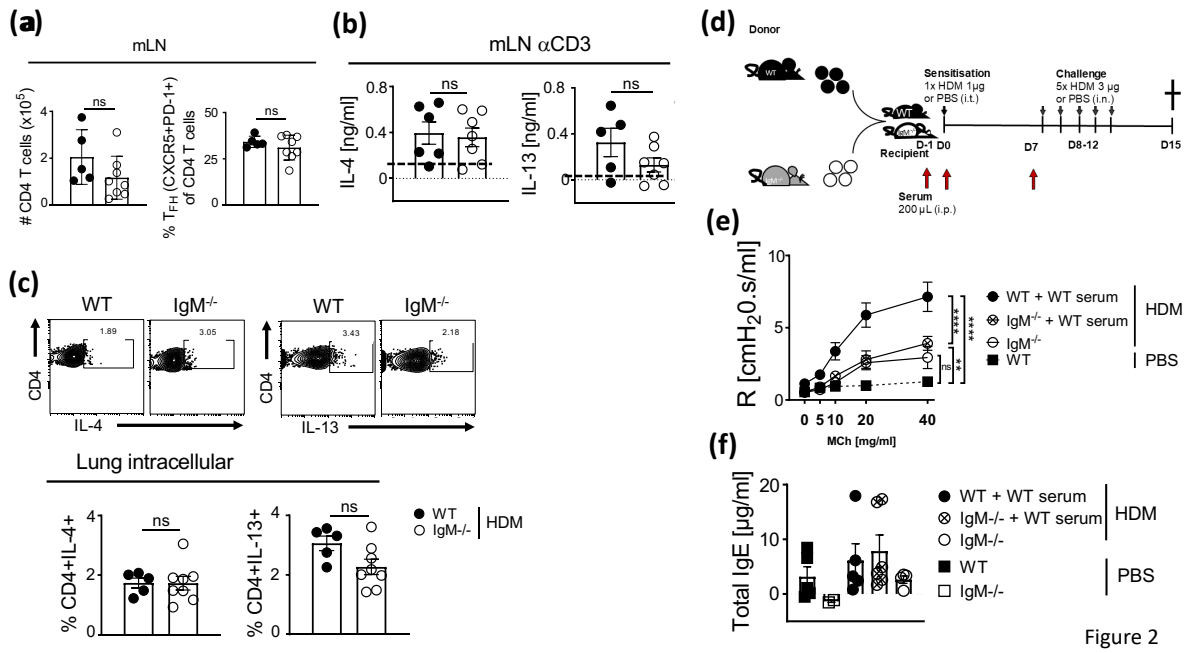

Figure 2

902

903 **Fig. 2 IgM-deficiency does not lead to reduced Th2 allergic airway inflammation**

904 **and serum transfer restores IgE, but not AHR.** Fig. a-c, mice treated as in Fig. 1a.

905 **a** Total mediastinal lymph node CD4 T cell numbers (live$^+$CD3$^+$CD4$^+$) and % of

906 Follicular Helper T cells (live$^+$CD3$^+$CD4$^+$PD-1$^+$CXCR5$^+$) of CD4 T cells were stained

907 and analysed by Flow cytometry and enumerated from % of live cells.

908 **b** Mediastinal lymph nodes were stimulated with anti-CD3 (10µg/mL) for 5 days and

909 supernatants were used to measure levels of IL-4 and IL-13. Cytokines were not

910 detected in unstimulated or HDM (30µg) stimulated mLN.

911 **c** Representative FACS plots and frequencies of lung CD4 T cells (live$^+$CD3$^+$CD4$^+$)

912 producing IL-4 and IL-13 after 5 hr stimulation with PMA/ionomycin in the presence of

913 monensin.

914 **d** Schematic diagram showing serum transfer from WT to IgM$^{-/-}$ which were then

915 sensitised as shown in Fig 1,a.

e Airway resistance was measured with increasing doses of acetyl methacholine (0 - 40 mg/mL).

f Total IgE in serum of mice either transferred with WT serum, $IgM^{-/-}$ serum or no serum.

Shown is the mean ± SEM from two pooled experiments (n=5 - 8). Significant differences between groups were performed by Student *t*-test (Mann-Whitney) (C, D, E) or by Tw*o-Way ANOVA with Benforroni post-test (B) and are described as: *p<0.05,* **p<0.01, ****p*<0.001, *****p*< 0.0001.

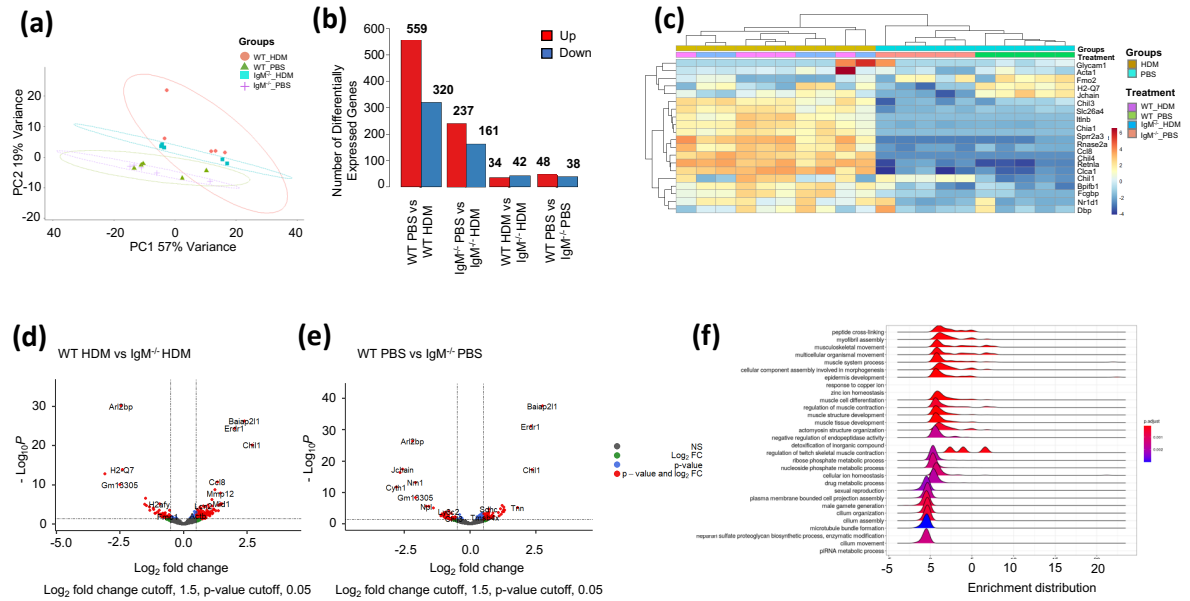

Figure 3

Fig. 3 Genes associated with muscle contraction are downregulated in IgM-deficient mice. WT and IgM$^{-/-}$ mice were treated as in Figure 1A and RNA was collected from the whole lung for RNA sequencing.

a Principal-component (PC) analysis showing variation in the global gene expression profiles across the different groups. PC1 (60%) and PC2 (18%), which capture the greatest variation in gene expression, are shown. Orange colour represents WT HDM, green colour represents WT PBS, Blue colour represents IgM$^{-/-}$ HDM and purple crosses represent IgM$^{-/-}$ PBS. Each dot represents an individual mouse.

b Number of differentially expressed genes between groups.

c Heatmaps depicting the differently expressed genes between WT and IgM$^{-/-}$ samples from HDM-treated and PBS mice ranked based on hierarchical clustering.

d-e Volcano plots: numbers and colour relate to genes that have an adjusted *p* value <0.05. Blue, significantly downregulated; red, significantly up regulated; grey, non-differentially expressed. P values were adjusted for multiple testing using the

Benjamini-Hochberg method. (D) represent changes between WT and IgM$^{-/-}$ treated with HDM and (E) represents changes between WT and IgM$^{-/-}$ treated with saline. **f** Gene set enrichment analysis (GSEA) of hallmark gene sets from the Molecular Signatures Database of the Broad Institute, showing the normalized enrichment scores (NES) for lung RNA-Seq data from WT mice.

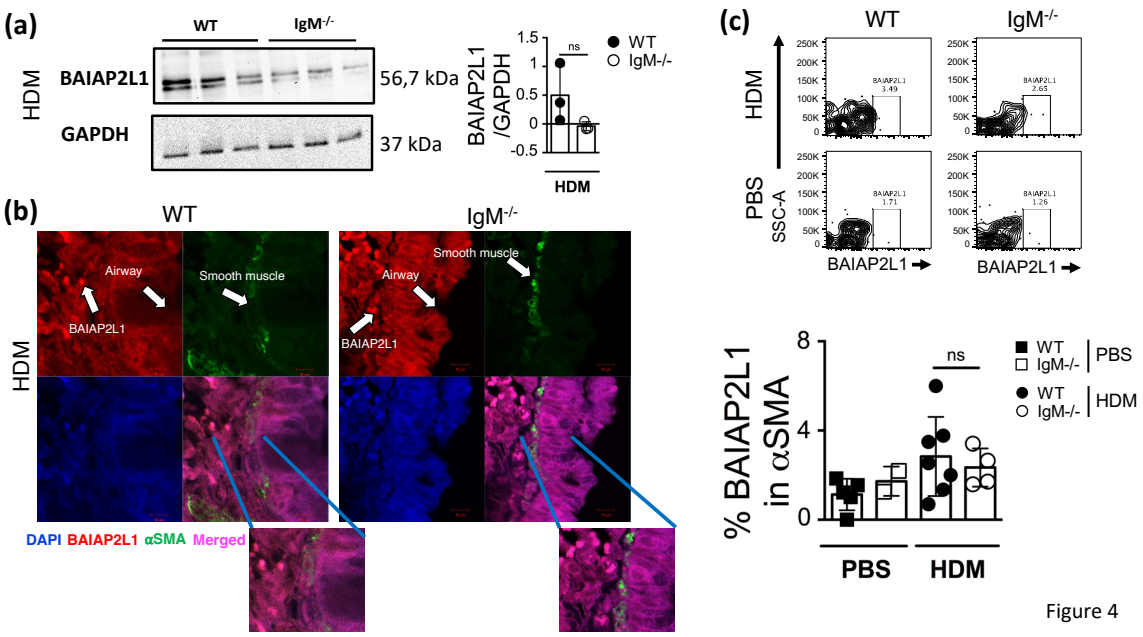

Figure 4

Fig. 4 *BAIAP2L1* is expressed in close contact to smooth muscle.

a Mouse lungs were homogenised in RIPA buffer and blotted on nitrocellulose. Rabbit anti-human BAIAP2L1 and mouse anti-GAPDH was used as primary antibody. Lines 1-3 is WT mice, lines 4-6 is IgM$^{-/-}$ mice sensitised and challenged with HDM.

b Lung sections from WT and IgM$^{-/-}$ mice sensitised and challenged with HDM were immunostained for nuclei stained DAPI (Blue), anti-BAIAP2L1 (red), α smooth muscle actin (green) and merged images (Magenta). Insert below shows zoomed in image of merged BAIAP2L1 and α smooth muscle actin.

c Representative flow cytometry plots showing BAIAP2L1 expression (Live^{+}Singlets^{+}CD45^{-}α SMA^{+}BAIAP2L1^{+}) in WT and IgM$^{-/-}$ treated with HDM or PBS. Quantification of % BAIAP2L1 in α smooth muscle actin is shown.

Shown are representative images from 2 independent experiments (n= 3 mice per group).

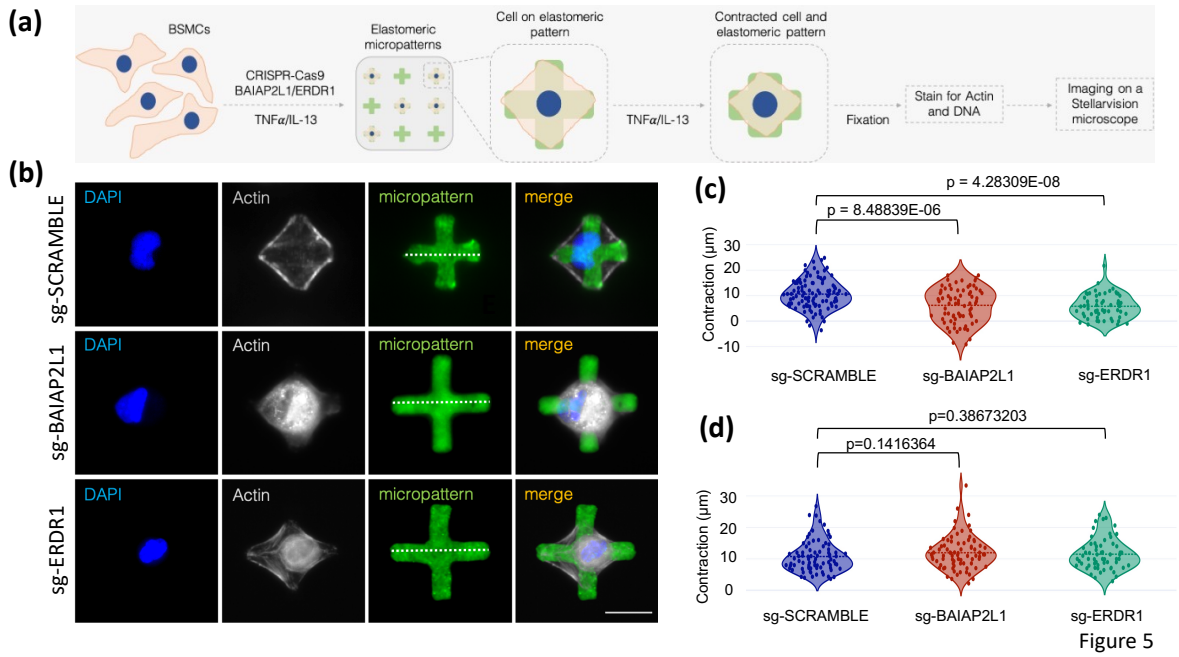

Figure 5

Fig. 5 CRISPR-based deletion of *BAIAP2L1* leads to reduced smooth muscle contraction at a single-cell level.

a, Bronchial smooth muscle cells ($1.6x10^5$ cells/well) were transfected with CRISPR-Cas9 single guide RNAs (scramble, *BAIAP2L1* and *ERDR1*), stimulated with recombinant human IL-13 (100 ng/mL) and TNF-α (10 ng/mL) for 48 h. Cells were then transferred to elastomeric micropatterns, stimulated again with rIL-13 and rTNF-α and fixed before imaging on a StellarVision microscope. **b**, Representative images of single BSMCs on micropatterns from scramble, *BAIAP2L1* and *ERDR1* stimulated with 10 ng/mL TNF-α. DNA was stained with DAPI, actin fibers with Phaloidin-565 and elastomeric micropatterns are coated in Fibronectin-488. Merged images are shown on the right. **c**, Violin plots showing contraction of 50-100 cells/condition stimulated with 10 ng/mL TNF-α, individual dots represent a single cell contraction, where blue is scramble sgRNA, red is *BAIAP2L1* sgRNA and green is *ERDR1* is sgRNA. **d**, Violin plots showing contraction of 50-100 cells/condition stimulated with 100 ng/mL

IL-13, individual dots represent a single cell contraction, where blue is scramble sgRNA, red is *BAIAP2L1* sgRNA and green is *ERDR1* is sgRNA.

Shown is mean ±SEMs from two pooled experiment (n=50 - 100). Significant differences between groups were performed by student t-test (Mann-Whitney) and *p* value is shown.

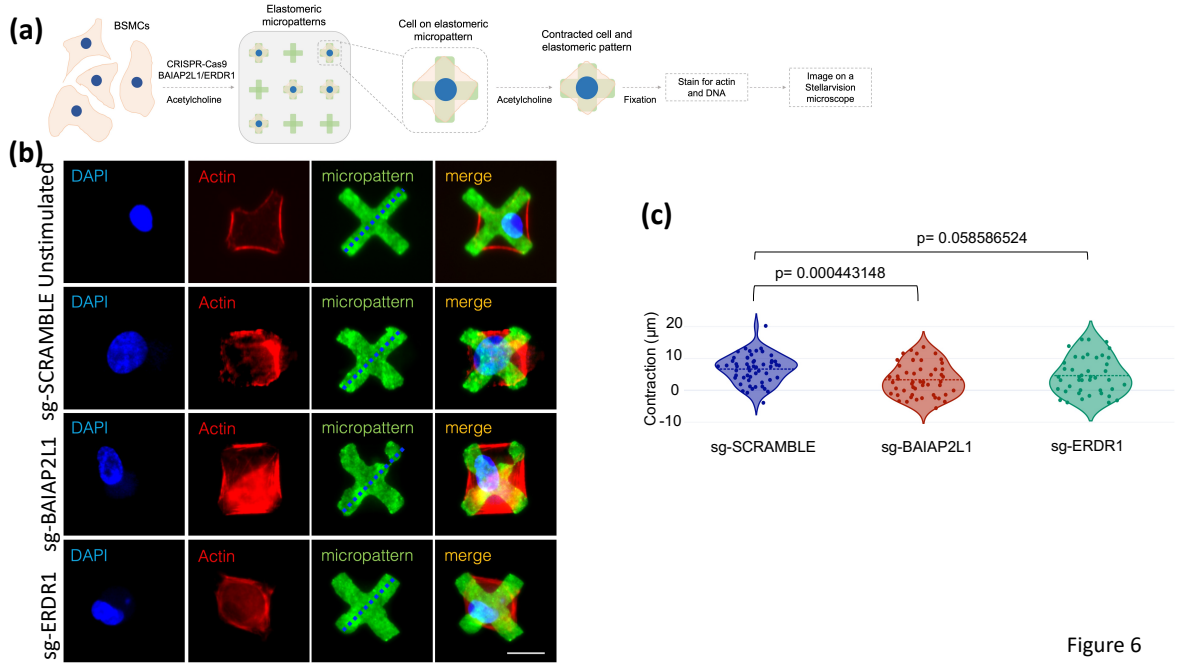

Figure 6

Fig. 6 CRISPR-based deletion of *BAIAP2L1* reduces smooth muscle contraction upon stimulation with acetylcholine.

a Bronchial smooth muscle cells ($1.6x10^5$ cells/well) were transfected with CRISPR-Cas9 single guide RNAs (scramble, *BAIAP2L1* and *ERDR1*), stimulated with Acetylcholine (10µM) for 48 h. Cells were then transferred to elastomeric micropatterns, stimulated again with ACh (10µM) and fixed before imaging on a StellarVision microscope.

b, Representative images of single BSMCs on a single micropattern from unstimulated, scramble, *BAIAP2L1* and *ERDR1* stimulated with ACh (10µM). Shown are DAPI, actin (red), a green fluorescent micropattern and merged images.

c, Violin plots showing contraction of 50-100 cells/condition stimulated with ACh (10µM) individual dots represent a single cell contraction, where blue is scramble sgRNA, red is BAIAP2L1 sgRNA and green is ERDR1 is sgRNA.

Shown is mean ±SD from 1 representative experiment of 2 independent experiments (n=50 - 100). Significant differences between groups were performed by student t-test (Mann-Whitney) and *p* value is shown.

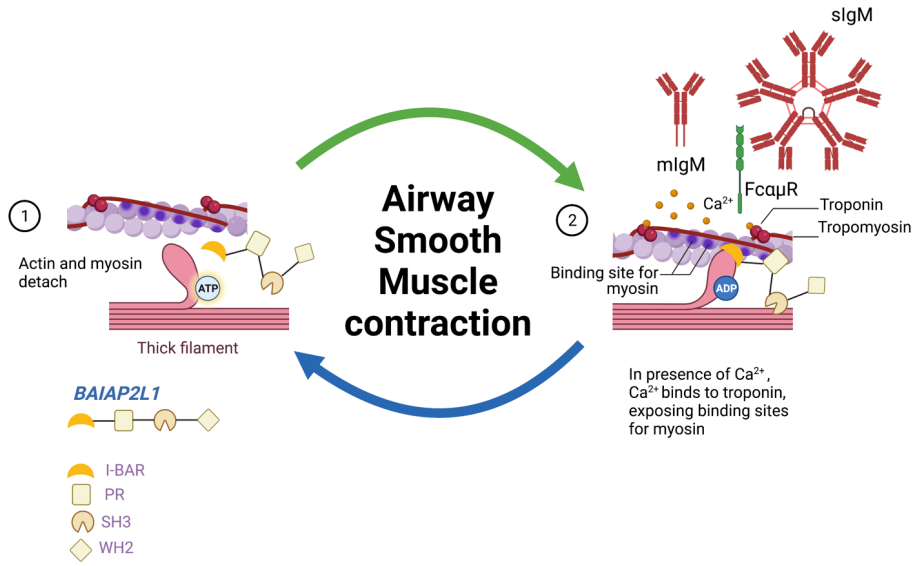

Figure 7

Fig. 7 Working model showing how *Baiap2l1* could influence muscle contraction through influencing myosin and actin filament interaction. Image adapted from Biorender.